Description of the UCam detector control system with a particular emphasis to a development of 4Kx4K camera systems

Nagaraja Bezawada*[a], Stewart McLay[a] and Derek Ives[b]
[a]UK Astronomy Technology Centre, Royal observatory, Balckford Hill , Edinburgh EH9 3HJ
[b]European Southern Observatory, Karl-Schwarzschild-Str. 2, 85748, Garching, Germany

ABSTRACT

This paper describes the features and functionality of the UCam (UKATC Universal Camera Control and Data Acquisition) detector control system with a particular emphasis on development and testing of two 4K x 4K CCD camera systems built recently at UKATC and delivered to a group of telescopes in India. These two camera systems use two variants of an e2v CCD203 device; a 4kx4k standard back-thinned device and a deep depleted silicon device. Apart from the expected differences with the spectral response of these devices, other performance differences have been observed between the two systems such as conversion gain non-linearity, electrical crosstalk between outputs, fringing etc. which are thought to be related to the silicon thickness. Both these detectors show charge trapping during device power on or when saturated. The effects of this charge trapping and a solution implemented to minimise it will be presented. The configuration of the UCAM system, custom built detector mount and fanout board and the overall performance of these camera systems will also be presented.

Keywords: UCam, CCD203, Astrocam, Conversion gain, Gradient, Charge trapping, Performance

1. INTRODUCTION

The UK Astronomy Technology Centre (UKATC) has recently built three standalone CCD camera systems for a consortium of telescopes in India. The camera systems were designed around the commercial off-the-shelf Astronomical Research Cameras, Inc. (ARC) controllers and in-house developed data acquisition software. Commercial off-the-shelf liquid nitrogen (LN) cryostats are used to cool the CCDs and custom fanout boards have been developed. One of the three cameras is integrated with an e2v CCD44-82 (2Kx4K) CCD whilst the other two cameras are fitted with e2v CCD203 (4Kx4K) standard silicon and deep depleted CCDs. This paper presents the features of the data acquisition software, implementation of the two 4Kx4K CCD camera systems and discusses the performance results.

2. THE UCAM DATA ACQUISITION SOFTWARE

2.1 UCam Software

The UKATC camera control and data acquisition system (UCam) operates under PC control, running Linux with a real time kernel, interfaced to a Generation-III ARC Controller. The system was originally developed for the very successful 3-colour high speed CCD photometer, ULTRACAM[1], designed and built at the UKATC for the Universities of Sheffield and Warwick, UK. The UCam system has been continually upgraded and used on many instruments developed at the ATC such as WFCAM, the largest wide field near IR camera in the world when commissioned and UIST, an imaging spectrometer at the UKIRT. The software has also been used in ULTRASPEC, a high speed spectrophotometer which uses an electron multiplication CCD. The UCam is also used on other instruments such as the FMOS, a fibre fed multi-object spectrograph at the SUBARU telescope and DAZLE built at IoA, Cambridge and used on GEMINI. It has recently been upgraded to a full commercial product as part of the development of a suite of CCD camera systems for delivery to a consortium of Indian telescopes. The following paragraphs describe the UCam system as implemented with the Indian Institute of Astrophysics (IIA) CCD camera systems.

The UCam[2] software runs on three HTTP server processes; Camera Control, File Save and Data De-multiplexer servers. The Camera Control server initialises, configures, downloads and executes applications. The File Save server handles the image data and writes to disk a meta-data file that also contains instructions how to sample and de-multiplex the raw.

*naidu.bezawada@stfc.ac.uk

High Energy, Optical, and Infrared Detectors for Astronomy IV, edited by Andrew D. Holland, David A. Dorn
Proc. of SPIE Vol. 7742, 77421A · © 2010 SPIE · CCC code: 0277-786X/10/$18 · doi: 10.1117/12.856960

image data. The De-multiplexer server de-multiplexes the saved data according to the instructions and implements the required data processing before saving the processed data in FITS file format. The UCam servers use HTTP as their communication protocol for easier integration into other systems. HTTP is a very common protocol that is widely supported by the most programming languages. Other software programs can communicate with the UCam system using the HTTP protocol. Examples of software are available in C/C++, Java and Python for interfacing with the UCam. Users can develop their interfaces in any environment and communicate to the servers using HTTP protocols. A user friendly GUI written in Python is also available which can be run remotely over the network or locally on the same host.

2.2 Features of UCam system

UCam is a real time data handling system which is limited only by the speed of the ARC Gen III controller itself. It has been proven with the ULTRACAM instrument to run at sustained data rates of > 20 Mbytes/second for a complete observing night. UCam also provides extendable post-processing capabilities. Typically for a CCD system this might only de-multiplex data coming from the controller. However for the IR detectors it can execute line fitting algorithms such as Fowler and up-the-ramp sampling, frame averaging, threshold limited integration and other complex image processing algorithms. It interfaces to DS9 or GAIA, an astronomical standard image display tools but can be extended to interface to other preferred image tools.

The software can be run remotely with a network connection to the host computer. For the fast data acquisition systems, the Ucam is run on a dedicated data acquisition PC with the graphical user interface (GUI) and the display tools running remotely on any other PC. Scripts can also be used to run the system without using the GUI. All the expected readout modes for CCD systems are supported such as binning, windowing, different readout speeds, different system gains etc. Test images can be generated for setup and debug purposes. These are generated in the CCD controller and then downloaded and displayed. Real time detector temperature monitoring support, usually from Lakeshore controllers, is also provided, but any other controller / monitor with an RS232 interface can also be supported. Temperature (up to 2 channels) is automatically logged into image FITS headers. User defined FITS headers can be automatically be updated on a frame by frame basis. The users can supply their own header input file which is picked up for each observation and written to the FITS image headers. Exposure controls such as pause/continue/extend and stop/abort are supported so that an exposure may be terminated, paused / continued with the resultant image file having the correct exposure time written to the FITS header. The exposure can also be aborted, for example frames with long readout time. Absolute time stamping to microsecond accuracy using a commercial GPS interface can be implemented. It also supports Record/Playback option where the user can record a sequence of commands by just clicking the appropriate buttons on the GUI. These commands are then written to an XML document where they can be played back later.

2.3 UCam desktop environment

A GUI client application called WxUCam is used for controlling the UCam server application. This application is written in the Python programming language and uses the wxPython cross platform GUI toolkit. At the moment wxPython supports 32-bit Microsoft Windows, most Unix or Unix-like systems, and Macintosh OS X platforms. Although at this time the UCam client application has only been tested on Linux and Windows platforms. An example of a desktop environment running WxUCam and IRAF is shown in Figure 1. In this example WxUCam, shown in the bottom left corner, automatically displays FITS images using the SAO astronomical imaging tool DS9. Users may reconfigure WxUCam to use other image display tools.

2.4 Camera application development

The UCam system does not use any high or low level software as supplied with the ARC controllers, directly from Astrocam. The drivers and the DSP code which runs on the PCI board and in the controller have been produced at the UKATC. This was done for many reasons but the main one was to ensure that the UCam system was reliable, especially at high speeds. The DSP application code is developed using ‘Freescale DSP56300’ assembly language and cross complier tools to produce a ‘common object file format’ (COFF) output file. Since the UCam uses XML format messages as its standard for communications, the COFF file is then converted into an XML document. An application, also described in an XML document, contains references to the corresponding configuration XML document (if parameters are associated with the application) or to the DSP object code XML document. The configuration file contains expressions and pre-check rules on the parameter values and describes the data output from the application such as number of readout channels, number of windows, size and format of the data etc. The selected application file is then parsed and the application DSP code is downloaded to the DSP in the controller. The DSP is loaded with an executable code for one application at a time. There can be several applications, one for each purpose, which can be selected to

download from the user interface. Each application can be configured with its own parameter values (such as exposure time, no. of exposures etc) before downloading to the DSP. Applications that just to do simple tasks such power-on or power-off the controller can have no parameters.

Codes have been developed to run many CCD types such as e2v 47-10, 47-20, 44-82, CCD201 (L3CCD), CCD203 and also to run infrared detectors such as Hawaii2, Aladdin-3 and Hawaii-1RG.

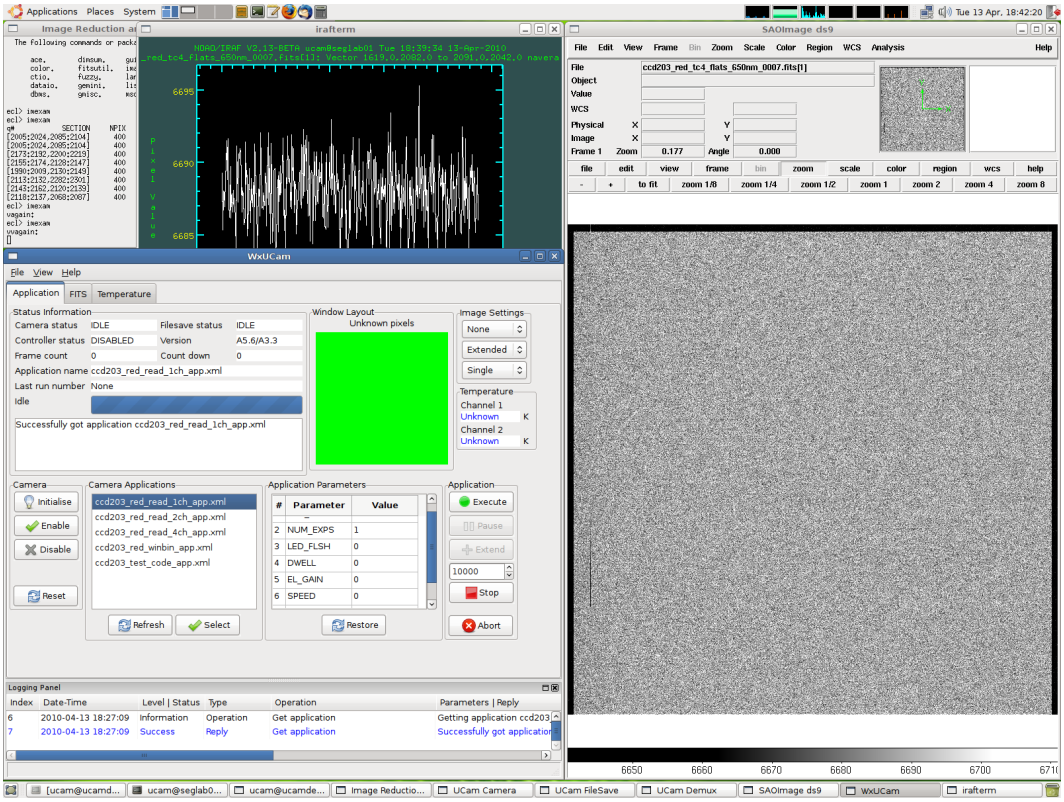

Figure 1: A screenshot of the UCam desktop environment.

3. CCD203 CAMERA SYSTEM

3.1 E2V CCD203

Two of the three camera systems have been integrated with the e2v CCD203[3] devices. One of the devices is a thinned standard silicon (~15um thick) with astro-broadband coating whilst the other device is a deep depleted silicon device (~40um thick) with an AR coatings optimized for red response. The CCD203 is a 4K x 4K, 12um pixels in a 2-edge close buttable package. The device has two serial registers; one at the bottom and one at the top of the array. The device has four readout amplifiers in total: two on each of the serial registers. The device offers flexibility such that it can be readout using any one or more output amplifiers simultaneously.

3.2 Camera controller

The camera controller is off-the-shelf generation-III ARC[4] controller with a standard timing board (ARC22), a clock board (ARC32) and a new 4-ch video processing board (ARC47) in a 6-slot housing assembly. The controller is interfaced with the host computer through a PCI interface board (ARC64). All the four readout amplifiers of the device are used and the user can select to read the frame through any one of the 4 outputs, the bottom 2 or the top two outputs or by using all the 4 outputs simultaneously. The ARC47 board has been configured to supply individual biases for each output amplifier. The CCD output signal is ac coupled to the input amplifier of the signal processing chain. The clock board generates two sets of parallel clocks to allow split operation of the parallel register. The corresponding serial clocks of both the serial registers are grouped together and hence the readout direction cannot be changed for each register independently. The output MOSFETs are provided with resistive loads to provide suitable drain currents.

3.3 CCD cryostat

Commercially available CCD cryostats from the Universal Cryogenics[5] have been used to house the CCDs. The cryostat is modular and has two sections; a cryo-module and a CCD head module. The cryo-module houses the LN reservoir surrounded by a vapour cooled radiation shield. The LN reservoir is rigidly supported to the back plate of the cryostat using G10 supports. The LN can is wrapped with aluminised Mylar sheet and the vapour cooled radiation shield with a multi-layer insulation in order to reduce the radiative heat load onto the LN reservoir. The radiation shield is also extended above the cryo-module onto the CCD head module to further reduce the heat load. A small container with activated charcoal getter is mounted directly on the LN can for sorption of residual and out gassed molecules.

The CCD head module consists of a temperature controlled stage supported from the front plate of the cryostat on to which the CCD mount is integrated. The temperature controlled stage is connected to the LN can via flexible gold plated copper straps which can be accessed through the two blank ports on the CCD head module. The temperature stage is electrically isolated from the rest of the cryostat to allow a separate ground control. The CCD mount temperature is controlled by a Lakeshore temperature controller using a heater resistor and a temperature sensor. An electromechanical shutter, controlled by a shutter controller unit, is directly mounted on the front plate of the cryostat.

A fan-out PCB is has been developed and located close to the CCD in order to provide over-voltage protection and ESD protection to the device. The PCB also includes bias filtering and clock shaping in order to provide a clean bias and clock inputs to the device.

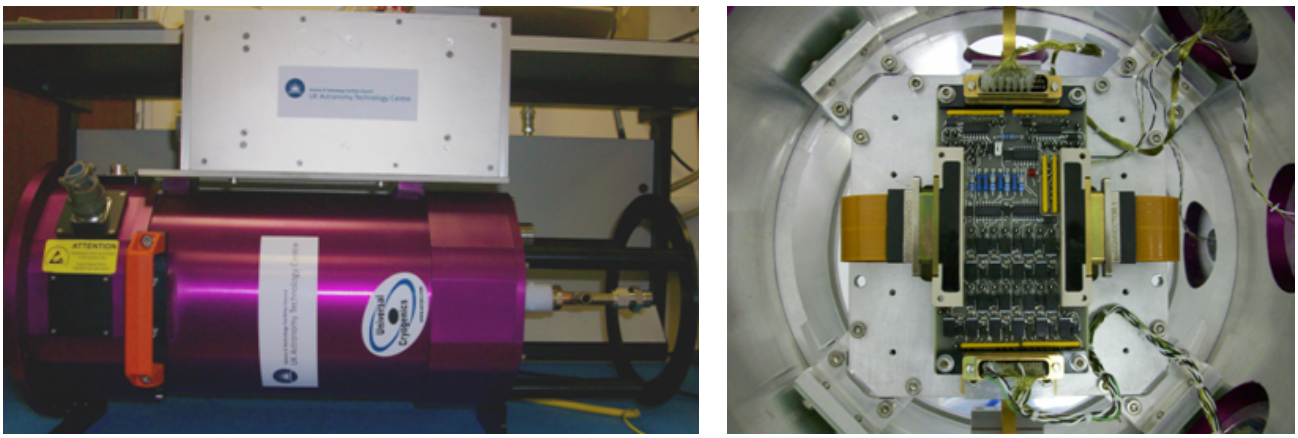

Figure 2: Left - CCD203 camera system with the ARC controller mounted on the cryostat; Right - Fan-out board for CCD203 – implements bias filtering, over voltage and ESD protection.

3.4 Camera readout applications

The CCD can be readout in full frame mode using three different applications: 1-channel; 2-channel and 4-channel applications. The readout times scale accordingly. Another application called ‘windowing and binning’ selects single output mode and allows to do pixel binning and window readout. Up to two non over-lapping windows and three bin factors are supported. The readout times are dependent on the window size, number of windows and also on the bin factors. The readout time for a full frame varies from a maximum of 100s using single output at low speed to a minimum of 20s using 4 outputs at high speed.

4. GENERAL PERFORMANCE

The characterization measurements have been carried out at ATC using our in-house test facilities. The facilities include a new large area uniform flat-field source and a calibrated quantum efficiency measurement system. Table 1 shows the general performance of the two camera systems. The flat-fields are obtained with 4-inch exit port integrating sphere at a distance of about 50cm from the CCD. The expected non-uniformity of the source at this distance is ~1%. Response uniformity is measured through three different narrow band filters centred at 400nm, 650nm and 950nm. The measured non uniformity at longer wavelengths is better for the deep depleted device compared to the standard silicon device. The deep depleted device as expected shows no signs of fringing at 950nm (FWHM ~10nm) whilst the standard silicon

device show fringing about 4.5%. In the case of the standard silicon device, the thin silicon substrate becomes transparent to the radiation and multiple reflections between the back and front surfaces of the substrate results interference fringes.

Table 1: General performance parameters of the two camera systems.

CCD Parameter	CCD203 Standard Silicon	CCD203 Deep Depleted
Read noise (170k pixels/s)	3.8e	4.4e
Full well	250ke	250ke
Dark Generation (@170K)	6.7e/pix/hr	5.1e/pix/hr
Non-linearity	1.04% (p-v)	0.20% (p-v)
Quantum Efficiency	See Figure 8	See Figure 8
Electrical Cross-talk *	0.02 – 0.08%	0.04 – 0.14%
Parallel CTE	0.9999999	0.9999999
Serial CTE	0.9999998	0.999995
Non uniformity	2.6%	1.6%
Fringing @950nm	4.5%	none

* - The electrical cross-talk between outputs is at its maximum between the two outputs on the same serial register. The cross-talk is at minimum between the diagonally opposite outputs. See Figure 12 for cross-talk images and text in section 5.3.

Table 2 shows the system gain and noise figures for all the combinations of electronic gain and speed settings that can be selected by the user for a readout application. The electronic gain setting defines the amplifier gain in the signal processing chain of the video processing board. There are up to 15 levels of gains selectable in the signal processing hardware, but only 3 settings are offered to the users which provide access to the full dynamic range of the CCD whilst sampling the readout noise adequately in most cases. The speed setting changes the electronic integrator sample time in the signal processing chain which changes the gain of the integrator and hence the frame readout time varies accordingly. Both these settings change the system gain (e/ADU). The system gain and read noise performance is similar for both standard and deep depleted devices indicating the sensitivity at the output amplifier for these devices is similar.

Table 2: Read noise performance the CCD203 standard silicon camera system.

Electronic Gain	Speed	System Gain (e/ADU)	Readout Noise
0	0	0.83	3.8
	1	1.66	6.1
1	0	1.61	4.0
	1	3.24	6.5
2	0	3.22	4.7
	1	6.45	9.0

4.1 Photon transfer non-linearity

The system gain is estimated using both photon transfer and Fe-55 methods for all the outputs. The system gain (e/ADU) is dependent on the speed and the electronic gain settings, which are user selectable. The system gain estimated using both the Fe-55 method and the photon transfer method at low signal levels agree very closely. However, the system gain estimated with the photon transfer varies with the signal level. Non-linearity in the conversion gain in CCDs was

reported earlier[6]. This has been attributed to an unknown mechanism of charge migration / interaction among the pixels in the imaging area proportional to the signal level. The effect of this charge interaction is the reduced point spread function and error in estimation of conversion gain using photon transfer. Both the standard silicon and the deep depleted devices have shown non-linearity in the photon transfer curve (Signal vs. Variance) as shown in Figure 3. However, the deep depleted device showed more non-linearity (~40%) than the standard silicon device (~15%). This can be directly attributed to the depletion depth in the silicon substrate. The more the depth of the well, the higher is the chance for migration to the neighboring pixels.

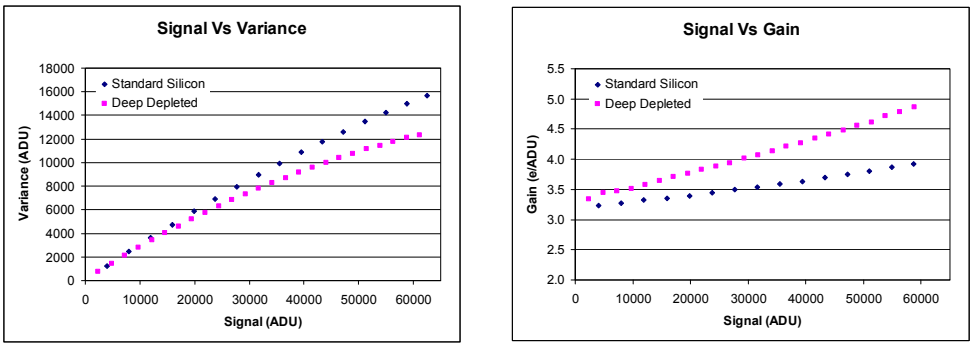

Figure 3: Photon transfer at different signal levels. Left - The slope of the photon transfer curve changes continuously with signal level. Standard silicon device show ~15% non-linearity whilst the deep depleted device shows non-linearity up to 40%. Right – Gain estimated from the photon transfer with signal.

4.2 Conversion gain issues

As mentioned earlier the change in the conversion gain with signal has been attributed to signal interaction among the pixels in the image area which dampens the shot noise. In order to verify this, pixels are binned on-chip in 2x2, 3x3 and 4x4 pixels and the gain is estimated using the photon transfer. With pixel binning, the signal level in the image area is kept low such that the binned signal did not saturate the serial register. Change in the conversion gain with signal is reduced dramatically with 2x2 pixel bins and it further reduced with 3x3 and 4x4 binning (Figure 4). The change in the conversion gain is almost negligible when pixels are binned 3x3 or more in both devices. This confirms that the charge spread is actually happening within the pixels in the image area. Therefore the conversion gain should be measured at low signal levels, but at signal levels sufficiently dominated by shot noise if the photon transfer technique is to be used.

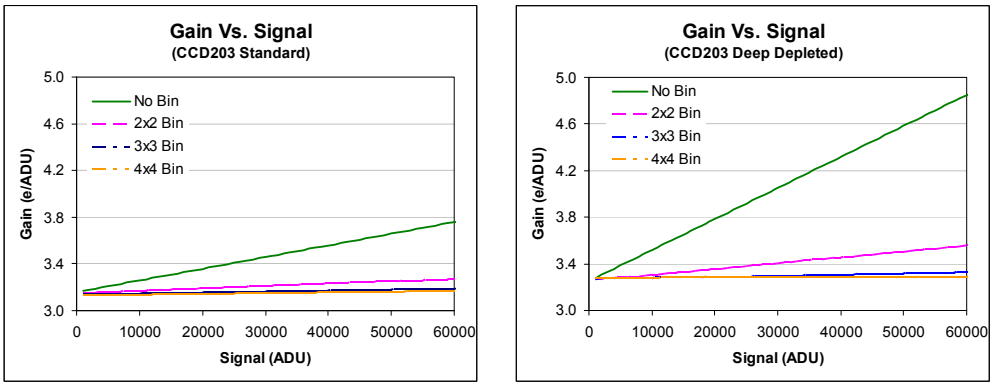

Figure 4: Gain measured using photon transfer with various pixel bin factors. For clarity only linear fit to the data are shown in the plots.

Spatial correlation analysis of the image data showed a strong correlation in the data with the deep depleted device compared to the standard silicon device. Figure 5 shows the sum of correlation of all neighboring 3x3 pixels with the signal level. Correlation in the 2x2, 3x4 and 4x4 binned data is almost negligible in both devices.

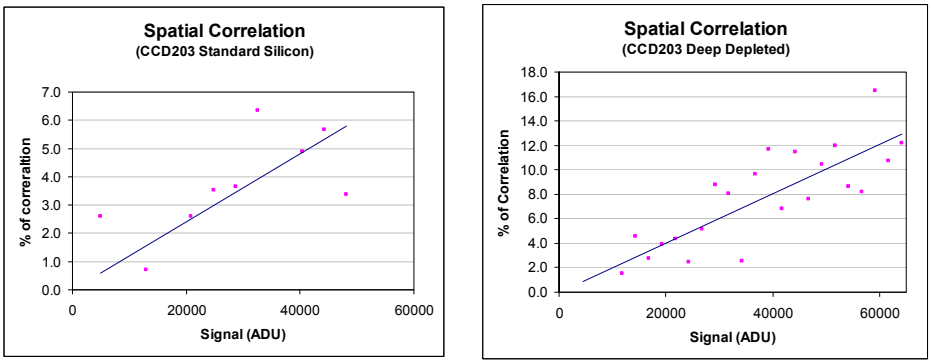

Figure 5: Spatial correlation of the image data. Deep depleted device shows a strong correlation compared to the standard silicon device.

4.3 Charge trapping

Both CCDs showed charges trapping as the devices are powered on. The bias and dark frames showed a gradient across the frame from bottom to top. The gradients reduced with time, but required more than an hour to stabilise. Also, the dark integration resulted in excess dark generation. This is because the charges trap in the interface states during power-on due to the changing electric fields. The trapped charge is then released slowly which results gradients in bias frames and excess dark generation. In both these devices, the parallel clocks are non-inverted for normal operation. Inverting the parallel clocks briefly during the power-on erases the trapped charges quickly and reduces the gradients. Figure 6 shows the bias gradients and excess dark generation with and without parallel inversion during power-on in the deep depleted device. Similar behavior is noticed with the standard silicon device also.

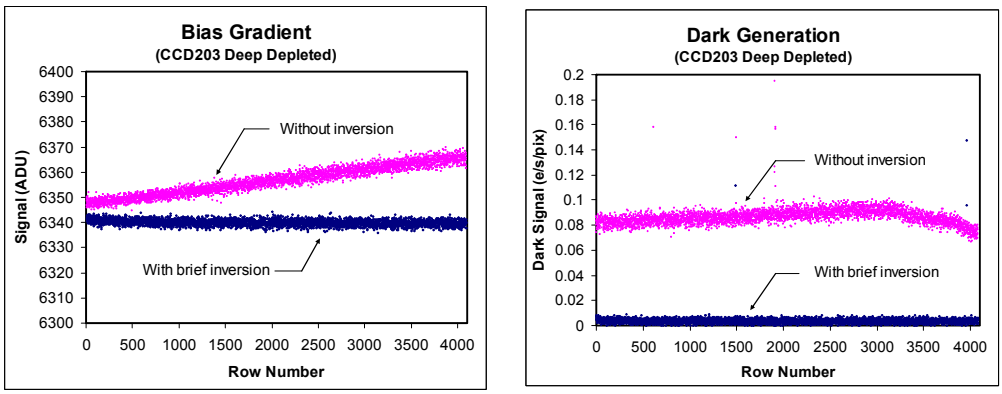

Figure 6: Left – Bias gradient after power-on without and with brief inversion. Right – Elevated dark generation measured after about 10minutes on power on. A brief inversion of the parallel clocks during power-on removes the trapped charges and reduces the effects.

4.4 Persistence due to saturation

The CCD when exposed to saturation, the charge starts interacting with the surface interface states and gets trapped. The trapped charge is then released during subsequent clocking leaving a trail of charge along the columns corresponding to the saturated pixels. This trapped charge contaminates the subsequent frames and can last for quite sometime. There is no such effect up until saturation, but once the saturation is reached, the charge starts to interact with the surface states with further charge integration. The harder the device is saturated, the more the charge trail is and the longer it lasts. The behavior is the same with both standard silicon and deep depleted devices. In order to get rid of the trapped charges, the parallel clocks are briefly inverted during the clearing of the CCD before starting the next exposure.

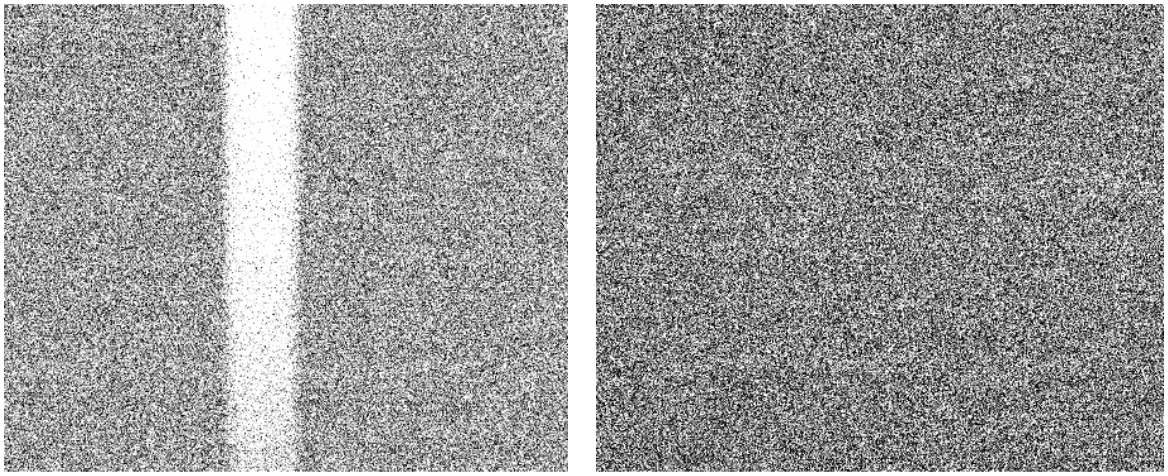

Figure 7: Left - Charge trail in the subsequent frame without inversion after saturating pixels with twice the well capacity; Right – Brief inversion of parallel clocks get rid of the charge trail.

5. PERFORMACNE DIFFERENCES

Apart from the above differences as described in the previous section, there are other performance differences between these two camera systems. These are discussed in the following sections.

5.1 Quantum efficiency

The quantum efficiency has been measured at discrete wavelengths using a scanning monochromator and different order sorting filters. The light from the exit port of the QE setup which under-fills a calibrated silicon photodiode is estimated using a pico-ammeter. The CCD is then used to integrate all the light seen by the photodiode from which the QE of the CCD is derived.

The QE of the CCD is measured at 170K and the plots are shown in Figure 8. The measured results agree closely with manufacturer test data for the blue device whilst ATC measured values are slightly higher for the deep depleted devices by about 10% in 500 – 700nm range. Conversion gain measured at low signal levels has been used to estimate the QE. The uncertainly is around 5% in these measurements.

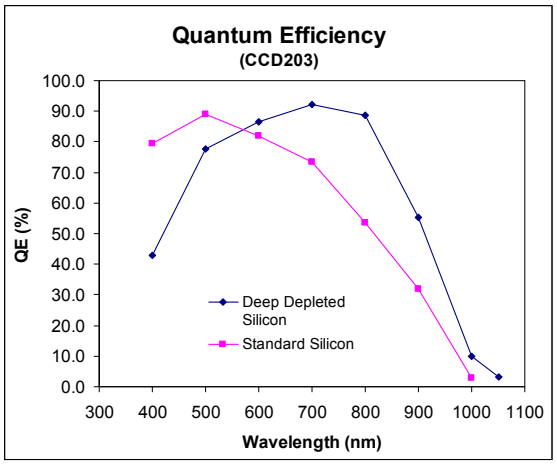

Figure 8: Quantum efficiency plots – measured values at ATC.

As expected, the deep depleted device show relatively high QE towards longer wavelengths compared to the standard silicon device, because the thick silicon is still opaque to the radiation even at longer wavelengths and hence there is a greater chance of interaction within the silicon. The device is also coated with anti-reflection coatings optimised for longer wavelengths to further improve the efficiency.

5.2 Charge collection and transfer

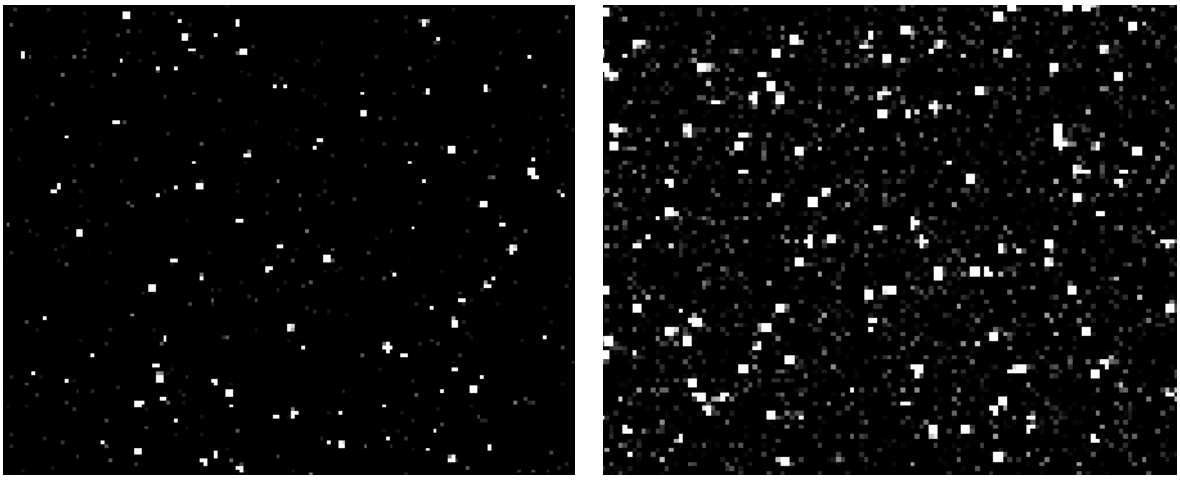

Figure 9: Fe-55 events. Left – Standard silicon CCD. Right - Deep depleted CCD. More split and partial events in the deep depleted device compared to the standard silicon device. The exposures are 5 minutes each.

Figure 9 shows part of the Fe-55 images. The x-ray events in the standard silicon appear sharper and have less split / partial events than in the deep depleted device. This is because the x-rays that are absorbed near the back surface diffuse more through the field-free region in the silicon and are collected by the neighboring pixels in the case of deep depleted device. This is also characterized by the increased pedestal level (corresponding to the split / partial events) in the event histograms shown in Figure 10.

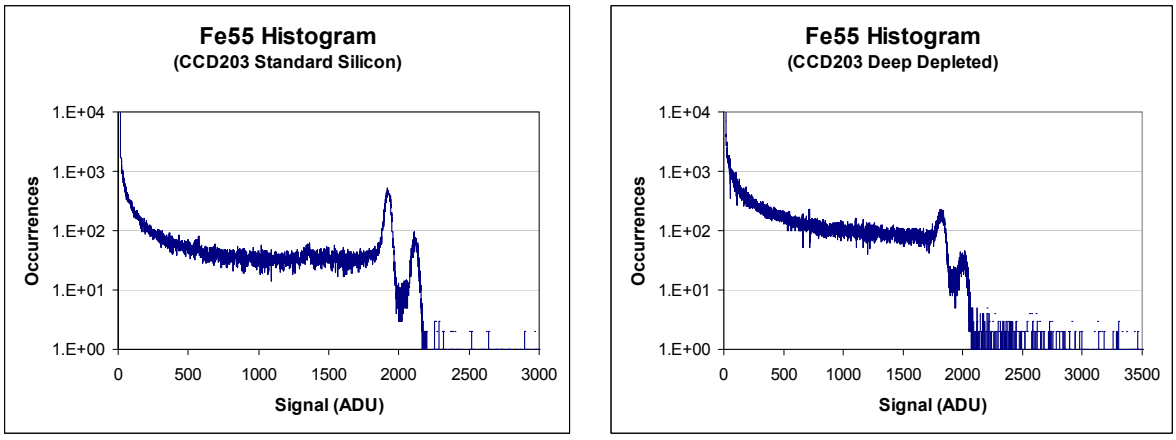

Figure 10: The escape peaks are sharper in standard silicon device. The more split / partial events seen in the deep depleted device (Figure 9) are evidenced by the increased pedestal level in the corresponding histogram.

Figure 11 shows the horizontal CTE maps for both standard silicon and deep depleted devices. As can be seen, the charge transfer is less efficient in the deep depleted CCD than the standard silicon device. Both serial registers in the deep depleted device showed similar CTE performance. The parallel CTE, however, remains excellent for these devices.

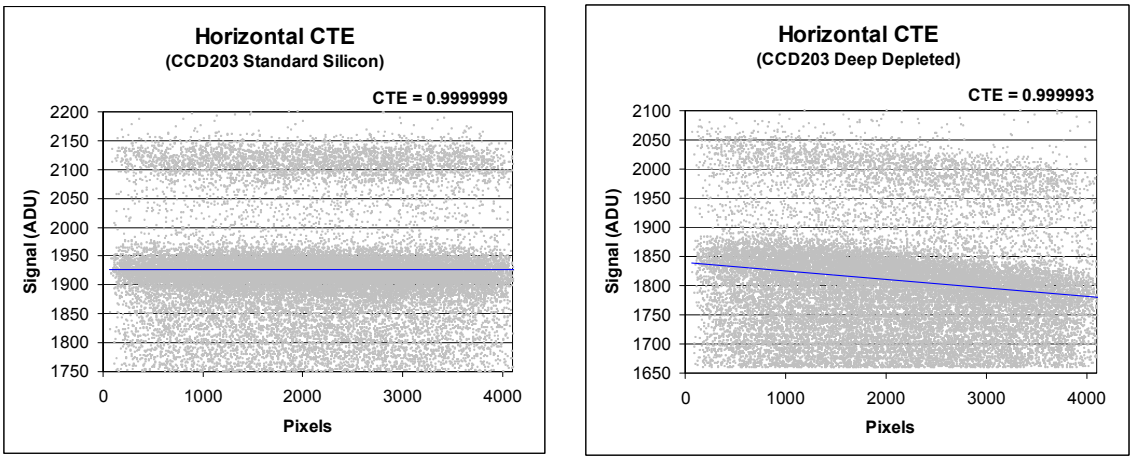

Figure 11: Horizontal CTE. Left – Standard silicon CCD. Right – Deep depleted CCD. The CTE in the deep depletion device is less efficient than in the standard CCD.

5.3 Electrical cross-talk

Both the camera systems exhibited cross-talk between the readout channels. When the device is read out using more than one output, a low level electrical cross-talk is seen between the outputs. Figure 12 (left) is a full frame image which shows ghost images through the other outputs when a spot is illuminated in the bottom-right quadrant. The cross-talk measured is different between different outputs as explained below. In the case of the standard silicon device, the cross-talk result in the bottom-left output due to the illuminated spot on the bottom-right quadrant (the near output in the same serial register) is about 0.08%. The cross-talk noticed in the top-right output (the near output on the other serial register) is about 0.03% and the cross-talk seen in the top-left output (the far output on the other serial register) is about 0.02%. The output amplifiers are supplied with individual bias supplies in order to minimize the cross-talk among the readout channels in the signal processing chain. It is believed that the origin for this cross talk is in the device. To confirm this, the position of the spot is changed from one quadrant to another Figure 12 (right) and the cross-talk pattern remained the same. That is, the cross-talk is always at its maximum between the outputs on the same serial register and is at a minimum between the diagonally opposite outputs. The cross talk may be reduced by having separate low impedance return signal paths for each channel right from the CCD to the controller[7]. Constant current loads on the CCD outputs may also improve the cross talk performance.

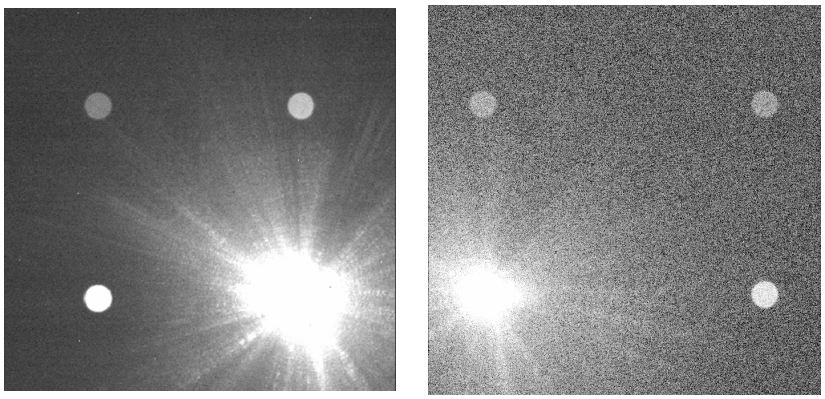

Figure 12: Electrical cross-talk between the outputs (standard silicon device) - Similar pattern is seen with the deep depletion device, but the cross-talk is slightly higher.

The cross-talk between the readout channels in the deep depletion is slightly higher than with the standard CCD. The pattern is similar to the standard silicon device. The cross-talk is about 0.14% in the other output on the same serial register and 0.09% to the near output on the other serial register and about 0.04% on the diagonally opposite output.

5.4 Cosmic ray events

The charge generated from the cosmic ray events is proportional to the length of their travel through silicon. Hence, the thicker the substrate, the longer the ionization radiation travels and more the interaction with the substrate. Hence the amount of charge detected and the number of pixels affected are more in the deep depleted CCD which is 40um thick compared to the standard silicon which is only of 15um thick. Most of the events in the standard silicon are with low counts whilst the events in the deep depleted device have tails of varying length, with higher counts.

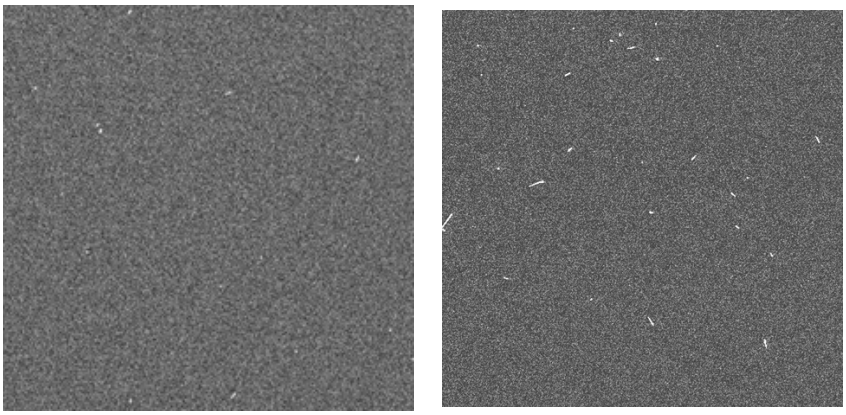

Figure 13: Cosmic ray events results more tails (attributed to the path length in silicon) – overall event rate is about 1.5events /min/cm^2 in standard silicon and about 2.5events/min/cm^2 in the deep depleted device. The window is made up of S1-UV fused silica.

5.5 Fringing

The thinned back illuminated, standard silicon device shows fringing when illuminated through a narrow band filter centered at 950nm (10nm FWHM). This is because, at these wavelengths the absorption depth in silicon becomes comparable with the thickness of the device and the substrate becomes transparent and effectively acts as a glass with two parallel surfaces. Multiple reflections between the two surfaces effectively cause interference fringes causing the modulations in the QE. Figure 14 (left) shows part of the flat-field from the standard silicon device. On the other hand there is no trace of fringing at the same wavelengths with the deep depleted device as the thick substrate is still opaque to the input radiation and hence no internal reflections (Figure 14 right).

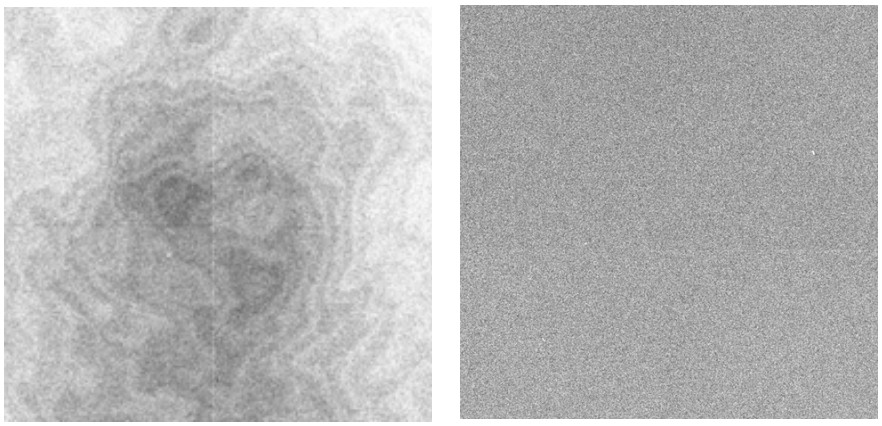

Figure 14: Left - Flats through 950nm narrow band filter show fringing ~4.5% in the standard device; Right - The deep depletion device shows no fringing at the same wavelengths.

6. CONCLUSIONS

This paper presented the features of the in-house developed UCam data acquisition software and the camera systems built around the ARC controller hardware. The CCD camera systems implemented using the UCam system are described. The general performance of the camera systems is presented and the performance differences between the two CCD203 standard silicon and the deep depleted camera systems are illustrated. Reasonably good performance is achieved with respect to noise, dark, linearity from both the camera systems. Both devices showed charge trapping during controller power on or after saturation. The trapped charge can be quickly removed by driving the parallel clocks into inversion briefly during power-on and during clearing frames. Both CCDs showed non-linearity in the photon transfer curve whilst their signal linearity remained excellent. Also, the non-linearity is much higher with the deep depleted device compared to the standard silicon device. The source for this appears to be in the image area where the charge collected under a pixel might be interacting with its neighboring pixels. This is further supported by the spatial auto correlation analysis of the image data where the correlation increased with the signal level. The correlation is also correspondingly higher in the deep depletion device. The Fe-55 X-ray events showed more partial / split events in the deep depleted CCD. The horizontal CTE is slightly less efficient in the deep depleted device whilst its parallel CTE is excellent. Both devices showed electrical cross talk between the outputs, but higher in the deep depleted device and it is believed that the origin for cross talk is in the device. Other performance differences between the two systems such as QE, fringing and cosmic ray events are also presented.

ACKNOWLEDGEMENTS

We would like express our thanks to Mr. K. Ravi, IIA (VBO, Kavalur) for supporting the systems post delivery, Prof. T. P. Prabhu and Mr. S. Sriram of IIA for discussions during the development of these camera systems. We would like to express our thanks to the workshop personnel and Brian Wilson at the UKATC for all the work they carried out for this project.

REFERENCES

1. Dhilon, V., Marsh, T. R., Kelly, J., Pashley, R., Stevenson, M., Atkinson, D., Beard, S., Ives, D., Peacoke, T., Tierney, C., Vick, A., "ULTRACAM -- an ultra-fast, triple-beam CCD camera," The Physics of Cataclysmic Variables and Related Objects, ASP Conference Proceedings, Vol. 261, p. 672 (2002)
2. McLay, S., Bezawada, N., Atkinson, D., Ives, D., "UCam: Universal camera control and data acquisition system," Proc. SPIE 7740 (2010)
3. http://www.e2v.com/products-and-services/imaging/space---scientific-imaging/datasheets/
4. http://www.astro-cam.com/
5. http://www.ucryo.com/
6. Downing, M., Baade, D., Sinclaire, P., Deiries, S., Christen, F., "CCD Riddle: a) Signal Vs. time: linear; b) Signal Vs. Variance: non-linear," Proc SPIE 6276, 627609 (2006)
7. Private communications with Dr. Bob Leach, Astronomical Research Cameras, Inc. Jun 2010.